J Mater Sci (2010) 45:3151–3159
DOI 10.1007/s10853-010-4320-z

Template and template-free preparation of one-dimensional metallic nanostructures

Stela Pruneanu · Liliana Olenic · Said A. Farha Al-Said · Gheorghe Borodi · Andrew Houlton · Benjamin R. Horrocks

Received: 11 December 2009 / Accepted: 12 February 2010 / Published online: 2 March 2010

Abstract In this article, we have studied and developed two approaches for organizing metallic nanoparticles into one-dimensional assemblies. The first uses DNA as a 'template' and allows the preparation of various silver nanostructures ('beads-on-a-string' or rod-like wires). The conductance of such nanostructures was demonstrated by employing a powerful technique, Electrostatic Force Microscopy (EFM). This technique gave us 'contactless' information about the electrical properties of silver nanostructures, aligned on a SiO_2/Si surface. Additionally, *I–V* characteristics of a single silver nanowire crossing two microelectrodes were recorded. The nanowire resistivity was estimated at 1.46×10^{-7} Ω m (at 300 K), which is one order of magnitude higher than that of bulk silver (1.6×10^{-8} Ω m). The second approach is a 'template-free' one, and exploits the binding ability of L-arginine, which favours the self-assembling of capped gold nanoparticles into gold nanochains. The results suggest that gold nanochains were formed due to dipole–dipole interaction between adjacent nanoparticles, which fuse together through an oriented attachment mechanism. Atomic force microscopy, TEM, UV–vis spectroscopy and X-ray diffraction were used to characterize the morphological, optical and structural properties of these metallic nanostructures.

S. Pruneanu (✉) · L. Olenic · G. Borodi
National Institute for Research and Development of Isotopic and Molecular Technologies, Donath Street 65-103, 400293 Cluj-Napoca, Romania
e-mail: stela.pruneanu@itim-cj.ro

S. A. Farha Al-Said · A. Houlton · B. R. Horrocks
School of Chemistry, Newcastle University, Bedson Building, Newcastle Upon Tyne NE1 7RU, UK

Introduction

There is currently a great interest in the preparation of hybrid materials from inorganic nanoparticles and biomolecules [1, 2]. One-dimensional (1-D) or two-dimensional (2-D) periodic arrays can be prepared in the presence of templates or coupling agents, such as DNA, surfactants and proteins. DNA has played an important role due to its molecular recognition capability. DNA-templated nanomaterials (metals, organic or inorganic semiconductors) are of particular interest in optoelectronics and biosensor devices [3]. Additionally, the high aspect ratio makes DNA an ideal template for creating electrical interconnects for microelectronics. The main problem to overcome is the high resistance of DNA [4, 5].

A practical approach often used to increase DNA conductivity is electroless plating, which involves the reduction of metal ions bound to DNA. By employing this method, silver [6–8], palladium [9], platinum [10], gold [11, 12] or copper [13] nanowires have been successfully created. Among these, silver has attracted a special attention due to its high electrical conductivity, which makes it an excellent candidate for incorporation in micro-electronics. Important aspects that were studied relate with the synthesis of nanostructures with controlled dimensions, morphology and chemical composition.

Berti et al. [14] reported a photography-derived methodology for fabrication of silver nanoclusters that entails exposing the Ag^+–DNA complex to 254 nm UV light for about 30 min. The complexation/photoreduction cycle was

repeated several times, until 'bumpy' structures of metal were observed along DNA. The side effect of this sequential procedure was the quick degradation of DNA, which leads to DNA shortening.

A different approach was used by Park et al. [15] who covered DNA by silver in a two-step metallization process, using glutaraldehyde-modified DNA. The diameter and uniformity of wires depend on the incubation time of DNA with glutaraldehyde as well as on the treatment with the initiator, $AgNO_3$.

Besides these methods, particular attention has been oriented towards preparation of 'template-free' 1-D nanostructures. This new approach is based either on a partial removal of the organic stabilization layer of nanoparticles [16] or in capping nanoparticles with certain amino acids. Zhong et al. [17–19] demonstrated the self-assembly of gold nanoparticles into chained networks, by using alkanethiols or amino acids as capping agents. Polavarapu and Qing-Hua [20] showed a single-step synthesis of gold nanochains, in the presence of stabilizers like glutamic acid and histidine. The results suggest that nanochains and nanowires were formed via the nanospheres fusing into one another, by an oriented attachment mechanism through dipole–dipole interactions.

The novelty brought by this work relates with the preparation of DNA-templated silver nanostructures with different morphologies (e.g. 'beads-on-a-string' or rod-like wires), which were easily produced only by varying the reaction time. The method employed by us was based on mixing Tollens reagent (diaminesilver(I) complex) with DNA solution (2.8:1 Ag^+/nucleotide). The reaction proceeds through a nucleobase redox process, due to the fact that the reduction potential of diaminesilver is higher than that of guanine base [21, 22]. Therefore, the reaction is thermodynamically favoured. We have qualitatively demonstrated the conducting properties of a single metallic nanowire aligned on a SiO_2/Si surface by using a powerful technique, Electrostatic Force Microscopy (EFM). Additionally, *I–V* characteristics at various temperatures (300–397 K) were recorded and the silver nanowire resistivity was obtained.

We have also developed a method for preparation of 'template-free' 1-D gold nanostructures by exploiting the binding ability of L-arginine. The zwitterionic properties of the amino acid create a net dipole moment on the nanoparticles surface, which favours the dipole–dipole interaction between adjacent nanoparticles. This leads to their subsequent fusion through an oriented attachment mechanism and formation of gold nanochains. The morphological, optical and structural properties of such metallic aggregates were investigated by TEM, UV–vis spectroscopy and X-ray diffraction method.

Experimental

Lambda DNA stock solution (500 μg/mL in 10 mM Tris–HCl pH 8 and 1 mM EDTA) was purchased from New England Biolabs, UK. Chloroauric acid ($HAuCl_4$), sodium citrate, sodium borohydride and L-arginine were obtained from Aldrich Chemicals and used as received.

Preparation of DNA templated silver nanostructures (*Ag–DNA*) is given in reference [23]. After preparation, they were aligned by molecular combing on SiO_2/Si surfaces, dried at room temperature for at least 1 h, and then investigated by Atomic Force Microscopy/Electrostatic Force Microscopy (AFM/EFM).

Arginine-capped gold nanoparticles (*Arg-GNP*) were prepared as follows: 1 mL L-arginine (0.075% in water) was added in 100 mL of $HAuCl_4$ (0.01%); after stirring the solution for about 5 min, 1 mL of reducing agent was added to the solution (0.075% $NaBH_4$). The solution was vigorously mixed again for another 5 min and kept at room temperature.

UV–vis spectroscopy: The optical properties of Ag–DNA and Arg-GNP solutions were monitored using an UV–vis spectrophotometer (JASCO V-570).

TEM measurements: For TEM analysis, drops of colloidal Arg-GNP solution were placed on carbon-coated copper grids. The drops were allowed to stand for 2 min and then the solution was removed with paper. The grids were further dried prior TEM measurements (JEOL-JEM 1010 instrument).

X-ray diffraction measurements were performed using a high-resolution Bruker D8 Advanced Diffractometer, with CuX-ray tube and incident beam Ge (111) monochromator ($\lambda = 1.54056$ Å).

AFM/EFM imaging was performed in air on a Dimension Nanoscope V system (Veeco Inc., Metrology group) using NanoProbe tips (Veeco Inc.). Vibrational noise was reduced with an isolation system (Manfrotto). All of the AFM images are height images taken in tapping mode, unless otherwise indicated. The SiO_2 surfaces were degreased by boiling the chips for 5 min in a series of solvents (trichloroethylene, acetone, isopropanol).

For *EFM* measurements, we have used MESP probes (n-doped Si cantilevers, with a Co/Cr coating, Veeco Inc.). These probes are 200–250-μm long, with resonant frequency around 79 kHz, quality factor (Q) between 200 and 260, and a spring constant between 1 and 5 N m^{-1}. In EFM measurements, an independently controlled bias was used to create an electrostatic field between the tip and the sample (the tip was grounded while the bias was applied at the sample). The images reported show the phase of the tip oscillation at a set lift height (50–70 nm typical) above the surface. In this mode, EFM has also been referred to as

'scanning conductance microscopy' because the phase is related to the force gradient and is sensitive to the conductance of nanowires as well as their polarisability.

Two terminal *I–V* characteristics of silver nanowire

Two gold microelectrodes were manufactured embedded in a SiO_2/Si substrate using standard photolithographic technique. Before aligning a single silver nanowire across the microelectrodes, silicon chips were treated with chlorotrimethylsilane (Me_3SiCl) vapour for about 15 min to reduce the surface wettability. Then, a 3-μL drop of Ag–DNA solution was deposited on the chip and spun with a spin-coater (300 rpm). After 1 min, the drop was removed from the surface, and the chip was let to dry at room temperature for at least 1 h.

The *I–V* curves for various temperatures (between 300 and 397 K) were recorded by placing the chip on a boron hot plate connected with a temperature controller West 6100. In order to avoid the conduction through surface impurities, a low bias was generally applied between the testing electrodes (±3 V). The current was measured using a Keithley 2400 instrument. Before each recording, the temperature was allowed to stabilize for at least 10 min.

Results and discussions

DNA-templated silver nanowires

The main analytical technique used to study DNA-templated nanostructures is AFM. This technique enables the shape and dimension of the prepared nanostructures to be imaged accurately. In combination with EFM [24, 25], it becomes a powerful tool to study the metallization process of DNA. Its importance arises from the acquisition of both morphological and electrical properties of a sample, in a single experiment. An easy distinction can be made between a bare DNA molecule (apparent height 0.5 nm, positive phase-shift in the EFM image) and that of a molecule covered by metal (diameter higher than 1 nm, negative phase-shift in the EFM image). In our case, it gives us 'contactless' observation of the conductance of Ag–DNA nanowires, aligned on a 220 nm SiO_2 oxide.

Our experiments have shown that Ag–DNA nanostructures with different morphologies can be produced only by varying the reaction time between DNA and Tollens' reagent (modified silver mirror reaction). The silver mirror reaction has been known for a long time [26], and in our case, it was conveniently modified in order to produce silver crystals along DNA strands. The driving force is the redox reaction between diamine silver(I) complex $[Ag(NH_3)_2^+]$ and guanine. The electrochemical reduction

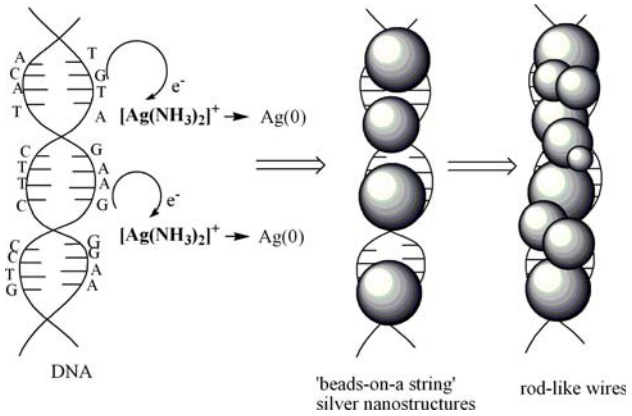

Fig. 1 Schematic illustration of the nucleobase redox process: formation of 'beads-on-a-string' silver nanostructures and rod-like wires

potential of diamine silver(I) complex (–0.4 V vs. Ag/AgCl) [21] is higher than that of guanine (−0.8 V vs. Ag/AgCl) [22] so the reduction of silver(I) complex by guanine is thermodynamically favoured (Fig. 1).

A short reaction time (less than 24 h) generally leads to the formation of silver nanocrystals, which are dispersed along DNA strands. Such 1-D nanostructures are presented in Fig. 2a, b, c and exhibit the characteristic 'beads-on-a-string' morphology (SiO_2/Si substrate).

Besides these, randomly dispersed silver nanocrystals from solution can be seen on the surface. Some DNA strands show parts, which are smoothly covered by silver (Fig. 2a) while others are densely packed with nanoparticles (Fig. 2b, c). It is interesting to emphasize that nanoparticles attached to DNA (mean diameter 30 nm, measured as height by AFM tip) are bigger than those randomly dispersed in solution (∼12 nm), which may suggest that the reduction of silver ions is catalysed by DNA.

In order to get information about the conducting properties of these nanostructures, we employed EFM technique or 'scanned conductance microscopy'. This is a dual technique, in which a dc bias is applied between a conductive tip and a SiO_2/Si substrate. The topography is recorded in the first pass, while in the second pass the tip is lifted at a certain height above the surface and the electric interaction between the tip and the nanowire is registered. As was previously reported for conducting wires (e.g. carbon nanotubes) [27–29], the phase of the tip oscillation in the second pass was negatively shifted. In contrast, for insulating or polarisable wires the phase was positively shifted. Although such study gives us only qualitative information, it is helpful for the evaluation of conducting properties of a single metallic nanowire, without the need to integrate it in a two terminal device.

The EFM images (phase) are presented in Fig. 2d, e, f (applied bias $V = -7$ V, lift height 50 nm). In these

images, Ag–DNA nanostructures appear as dark lines, the dark area being larger than their AFM width, due to the long range electric interaction. Although the AFM images show that Ag beads attached to DNA are disconnected, all the EFM images confirm that in fact they form continuous conducting paths (Fig. 2d, e, f). This means that the DNA wire connecting the beads has been covered by metallic silver. This is in contrast with randomly dispersed silver nanoparticles on SiO_2 surface, which show a bright contrast (positive phase-shift). Also, bare DNA strands show a positive phase-shift, confirming its insulating character (data not shown).

When the incubation time of Tollens' reagent and DNA was much longer (about 3 days at room temperature), rod-like nanostructures were generally produced (Fig. 3a, b, c). The AFM images show that the DNA template was uniformly covered by silver. The mean diameter of the new nanostructures was considerably larger than that of bare DNA strands (e.g. mean diameter 75 nm, Fig. 3c). The formation of such uniform and conducting wires follows the Ostwald ripening process, at the expense of small silver nanoparticles unattached to DNA.

The EFM images (applied bias $V = -7$ V, lift height 50 nm) recorded for these Ag–DNA nanostructures are

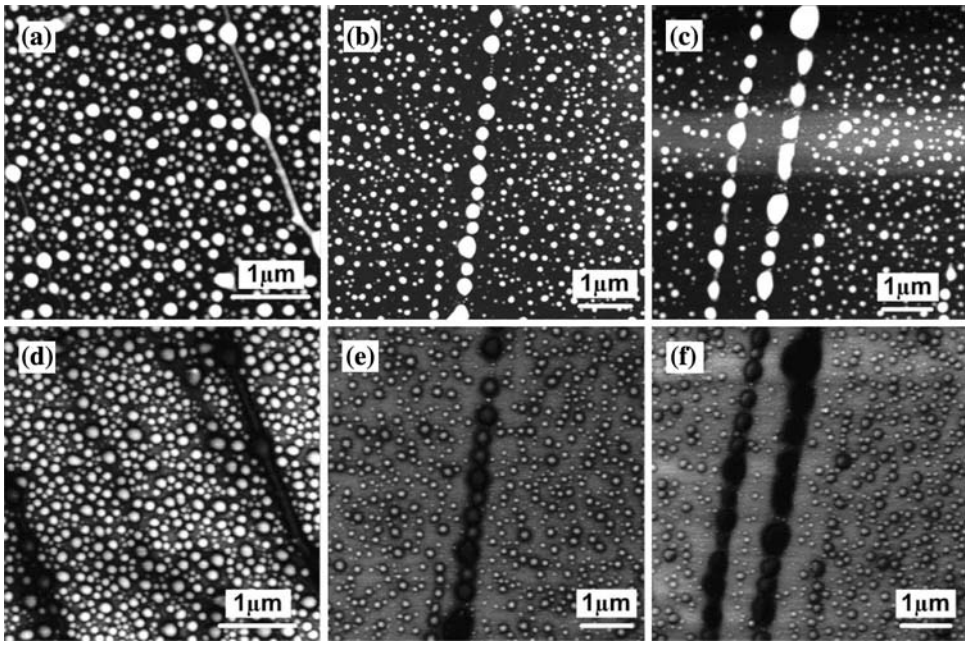

Fig. 2 Tapping™ mode AFM images of silver 1-D nanostructures on a SiO_2/Si surface (**a**, **b**, **c**); corresponding EFM phase images at a bias of −7 V and 50 nm lift height (**d**, **e**, **f**)

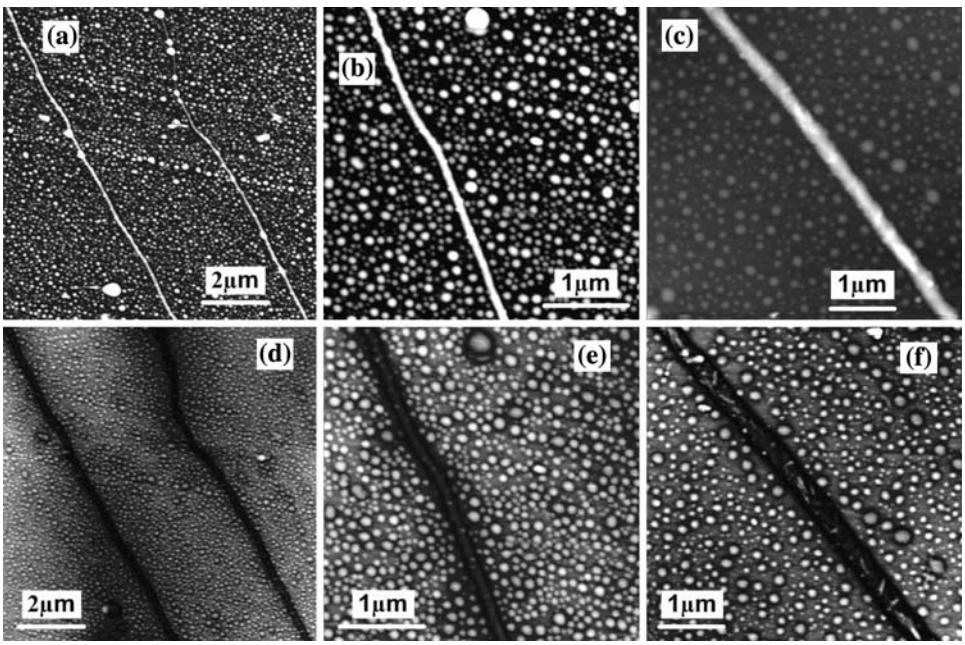

Fig. 3 Tapping™ mode AFM images of Ag–DNA wires on a SiO_2/Si surface (**a**, **b**, **c**); corresponding EFM phase images at a bias of −7 V and 50 nm lift height (**d**, **e**, **f**)

similar with those presented before: the rods appear as dark lines while the randomly spread silver crystals as bright spots. A parabolic dependence of the phase-shift on tip-sample bias was observed for all prepared Ag–DNA nanostructures, although a small asymmetry was sometimes present due to trapped charges in silver crystals. Thicker nanowires (mean diameter $d = 45$ nm) have a significantly larger phase-shift than thinner nanowires ($d = 12$ nm), which indicates a higher conductance (data not shown).

We next performed two terminal *I–V* measurements of a single silver nanowire connecting two gold microelectrodes. Figure 4 shows the AFM topography of such nanowire. The length of the wire is around 9 μm while the diameter is about 16 nm (measured as height in the AFM image). Some impurities from Ag–DNA solution are also present on the SiO_2 surface, partly covering the nanowire.

The variation of *I–V* characteristic with the temperature is presented in Fig. 5a, b. As a general trend, we can notice that the current increases with the temperature. A background current was also recorded for the clean electrodes (no nanowire attached) and this was significantly lower, 10^{-8} A. At room temperature (300 K), the *I–V* curve is linear (Fig. 5a), while at higher temperatures (between 307 and 337 K), the nanowire exhibits a semiconducting behaviour with a slight deviation from linearity. At even higher temperatures (357 K), a sudden decrease in the current was observed, and the curve linearity was restored (Fig. 5b). Most probably such a behaviour was caused by an oxide or a contamination layer, which was destroyed by the temperature increase. A further increase in current was obtained at 377 and 397 K, respectively.

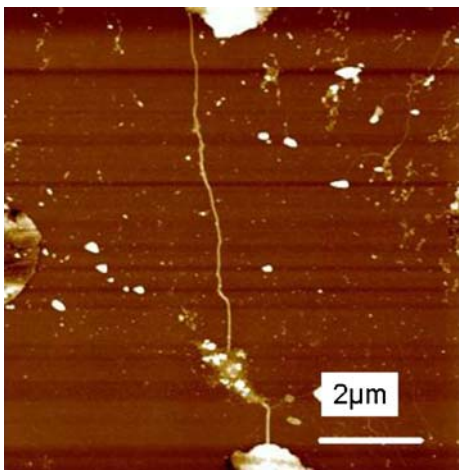

Fig. 4 Tapping mode™ AFM image of a single Ag–DNA nanowire connecting two gold microelectrodes (nanowire length $L \approx 9$ μm, average diameter $\approx$ 16 nm); height scale 30 nm

The nanowire resistance was calculated from the linear part of *I–V* curve (at 300 K), and a value of 6,580 Ω was obtained. From this value, the nanowire resistivity was estimated at 1.46×10^{-7} Ω m, using a nanowire length of 9 μm and a radius of 8 nm. Such a value is one order of magnitude higher than that of bulk silver (1.6×10^{-8} Ω m) but this is not surprising due to the presence of oxides or contaminants, which alter not only the electrical properties but also prevent the formation of an adequate contact between the nanowire and the gold electrodes. This is additionally supported by our XRD and XPS results (data not shown), which confirmed that the composition of the nanowire is a mixture of Ag and Ag_2O.

Gold nanochains formed by self-assembly of L-arginine-capped nanoparticles

One-dimensional metallic nanostructures can be produced in the absence of an extraneous template by exploiting the binding ability of L-arginine. TEM images show that after preparation, arginine-capped gold nanoparticles agglomerate into large spherical or elliptical aggregates (diameter between 10 and 50 nm, Fig. 6a, b). By careful examination of Fig. 6a, one can see that inside the large particles there

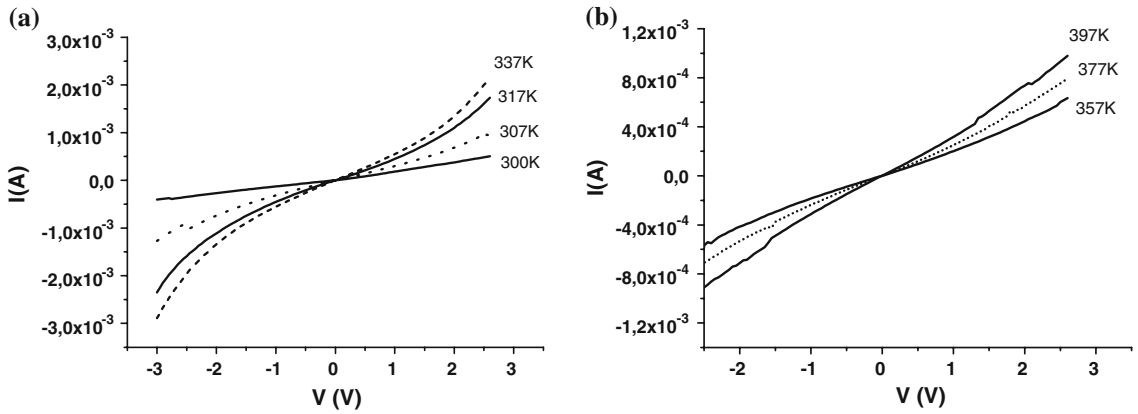

Fig. 5 Temperature dependence *I–V* curves of a single Ag–DNA nanowire aligned between two gold microelectrodes

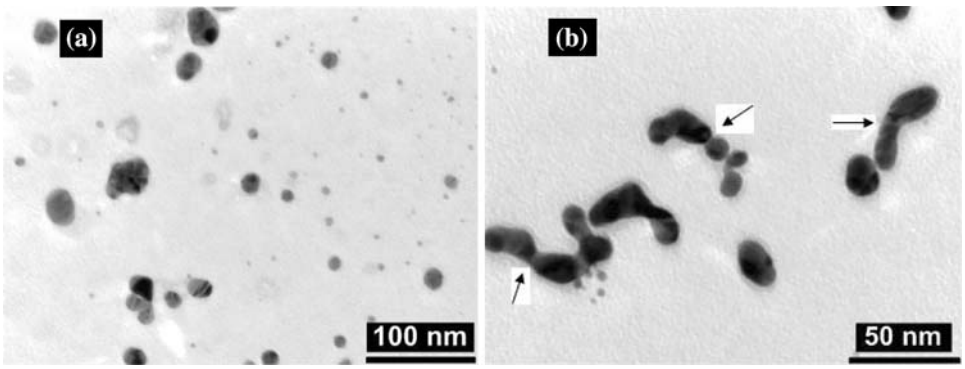

Fig. 6 Arginine-capped gold nanoparticles, immediately after preparation (**a**); 1 h after preparation (**b**)

are pairs of lines, which have also been reported in gold crystals synthesized by polypeptides [30]. These lines may be attributed to the presence of multiple twinned crystals, formed by the fusion of smaller ones sharing the same lattice plane [31, 32]. Figure 6b shows the presence of peanut-shaped gold nanocrystals, formed by the fusion of two or more nanoparticles in such a way that the boundary lattice plain match each other (see the arrows). These peanut-shaped particles will subsequently connect with other nanoparticles forming chain-like structures.

Within 3 h after $NaBH_4$ was added to the solution highly extended 1-D nanostructures were produced, having branches or closed loops of various lengths (Fig. 7a–f). This morphological change was also accompanied by a colour change, from pale pink to pale blue. The cross-sectional wire diameter is close to that of elliptical aggregates (between 10 and 50 nm) while the length ranges from tens to hundreds of nanometres. One can notice from place to place individual Au nanoparticles, interconnected with their neighbours due to L-arginine cross-linking ability. After a longer period of time (48 h, Fig. 7e, f), less dispersed gold nanoparticles can be seen in the TEM images, which indicates that an increasing number of linear assemblies were formed. In particular, Fig. 7d, f show that the particles are well fused into each other.

The optical properties of metallic nanoparticles (silver, gold or copper) rely on a strong absorption band in the visible spectrum, called the plasmon band [32]. Mie theory shows that for a small sphere the light absorption is given by a single surface plasmon resonance band (SPR), which is due to a dipolar charge distribution on the surface (transverse SPR) [33]. As the particles assemble into extended anisotropic nanostructures (chains and branches), the charge distribution induced on the surface can result in dipolar modes, with different resonant frequencies. Consequently, an additional SPR band is developed, generally red shifted (longitudinal SPR).

This change was clearly observed in the UV–vis spectra of arginine-capped gold nanoparticles (Fig. 8). Immediately after preparation (20 min), the spectrum of Arg-GNP is that characteristic for dispersed nanospheres, having a single plasmon peak at around 530 nm. This corresponds to transverse surface plasmon vibrations in arginine-capped gold nanoparticles. The peak intensity increases for the next 2 h, indicating that more capped nanoparticles are formed in solution. Marked changes occur in time (24 h) due to the self-assembly of nanoparticles into nanochains (peak broadening accompanied by a strong decrease in intensity).

The self-assembly is favoured by the binding ability of L-arginine, a polar amino acid. At pH 5, the α-amine group (pK_a 9.09) and the side chain amine group (pK_a 13.2) are protonated (positively charged) while α-carboxylic groups (pK_a 2.18) are partly dissociated (bearing negative charges). In this case, gold particles can easily connect to the terminal amine group. The linking via α-amine group is not favoured due to the repulsion between GNP and the polar carbonyl group in amide. This leaves protruding the α-groups (amine and carboxylic), which can create a net dipole moment on the nanoparticle surface. As already reported, the presence of an intrinsic or induced dipole moment led to the assembly of colloidal nanoparticles into nanochains [34]. TEM images and UV–vis spectra recorded at different stages of the reaction confirmed that immediately after preparation, dispersed nanoparticles were formed followed by their aggregation into nanochains. In addition, there was a significant reduction in the number of small particles, as TEM images revealed.

According to the literature, the formation of gold nanochains takes place by an oriented attachment mechanism [20, 35]. This describes the spontaneous attachment of two neighbouring particles, sharing a common crystallographic plane.

Figure 9 shows the X-ray powder diffraction pattern of arginine-capped nanoparticles. The peaks were assigned to the diffraction from the {111}, {200}, {220}, {311} and {222} planes of fcc gold crystal.

The theoretical and experimental intensity of the diffraction peaks are normalized at the highest values and are presented in Table 1.

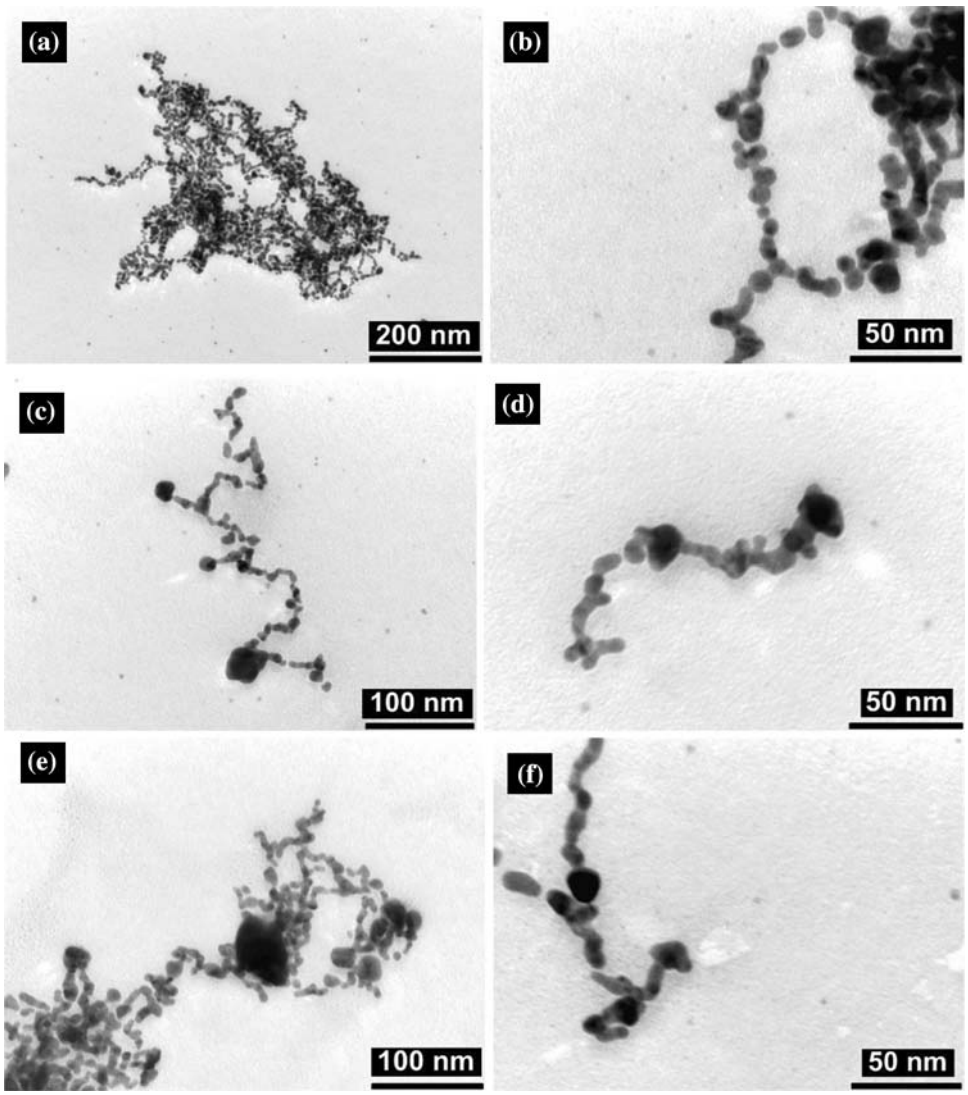

Fig. 7 Arginine capped gold nanoparticles: **a**, **b** 3 h after preparation; **c**, **d** 24 h after preparation; **e**, **f** 48 h after preparation

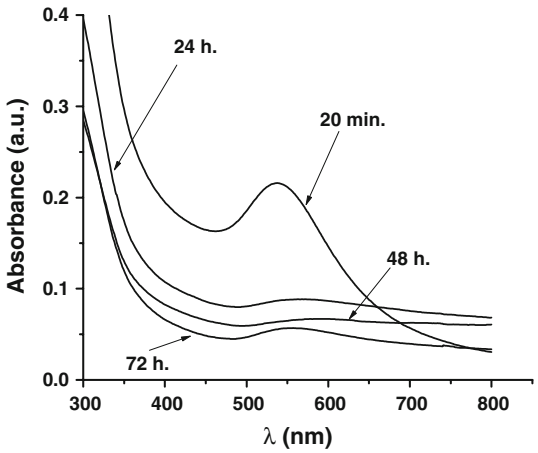

Fig. 8 Evolution of UV–vis spectra in time, for arginine-capped gold nanoparticles

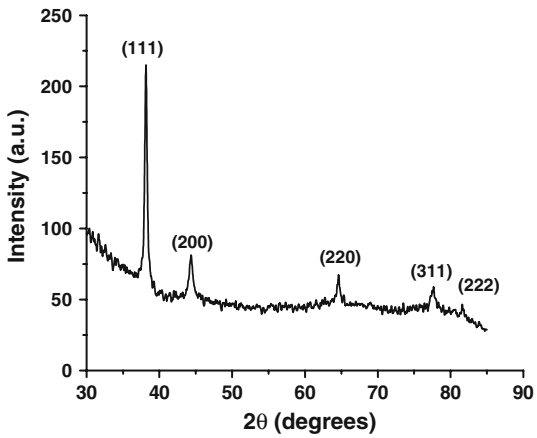

Fig. 9 X-ray powder diffraction pattern of arginine-capped nanoparticles

Table 1 Theoretical and experimental intensities of the diffraction peaks

Crystal planes	Theoretical	Experimental
{111}	100	100
{200}	45.5	19.5
{220}	23.9	13.4
{311}	24	11.7
{222}	6.7	6.8

As can be seen in Table 1, the intensities of {200}, {220} and {311} experimental peaks are lower than their theoretical values. This confirms that arginine-capped gold nanoparticles are mainly dominated by {111} facets. In addition, the high intensity of the {111} planes implies that they are preferentially oriented parallel to the surface of the supporting substrate, on which the gold nanochains are lying. Based on this observation, we can conclude that the growth direction of gold nanochains is parallel to Au {111} planes. As well known from the X-ray powder diffraction, the Au {111} facets have many equivalent planes, e.g. (−1, 1, 1), (1, −1, 1), (−1, −1, 1), etc. These equivalents planes are oriented almost perpendicular to {111} facets (having an angle of 70.53 or 109.47 degrees).

The affinity of amine group for {111} facets (or their equivalent planes) is relatively weaker compared to other facets [36]. Consequently, the {111} equivalent planes are not covered by the terminal amine groups belonging to L-arginine molecules, being available for nanoparticles fusion. This subsequently leads to the formation of gold nanochains.

Using Sherrer equation, the mean crystallite dimension was calculated from the diffraction breadth. The crystallite dimension perpendicular to the {111} plane was $D_{111} = 311$ Å, and the crystallite dimension perpendicular to the {200} plane was $D_{200} = 227$ Å.

Conclusions

In conclusion, we have shown that 1-D metallic nanostructures can be easily produced, using biomolecules either as a template or as a capping agent. DNA-templated silver nanostructures can have various morphologies, e.g. 'beads-on-a-string' or rod-like wires, depending on the reaction time. All these nanostructures have conducting properties, which was qualitatively demonstrated using EFM. The resistivity of a single silver nanowire, estimated from *I–V* curve (300 K) was one order of magnitude higher than that of bulk silver.

Gold nanochains were produced in a single-step synthesis, in the presence of a reducing agent ($NaBH_4$) and using L-arginine as capping agent. TEM and UV–vis measurements have confirmed that gold nanospheres were formed in the first stage of preparation but they self-assemble into nanochains. The nanochains were formed by an oriented attachment mechanism, through the fusion of nanospheres, which were mainly dominated by {111} facets.

Acknowledgements The National Authority for Research Romania, One NorthEast UK, EPSRC UK, the government of Saudi Arabia and the EU are thanked for the funding.

References

1. Stoltenberg RM, Woolley AT (2004) Biomed Microdevices 6(2):105
2. Gu Q, Cheng C, Gonela R, Suryanarayanan S, Anabathula S, Dai K, Haynie DT (2006) Nanotechnology 17:R14
3. Storhoff JJ, Mucic CR, Mirkin CA (1997) J Cluster Sci 8:179
4. Porath D, Bezryadin A, de Vries S, Dekker C (2000) Nature 403:635
5. Rakitin A, Aich P, Papadopoulos C, Kobzar Y, Vedeneev AS, Lee JS, Xu JM (2001) Phys Rev Lett 86:3670
6. Braun E, Eichen Y, Sivan U, Ben-Yoseph G (1998) Nature 391:775
7. Keren K, Krueger M, Gilad R, Ben-Yoseph G, Sivan U, Braun E (2002) Science 297:72
8. Deng ZX, Mao CD (2004) Angew Chem Int Ed 43:4068
9. Richter J, Seidel R, Kirsch R, Mertig M, Pompe W, Plascheke J, Schackert HK (2000) Adv Mater 12:507
10. Ford WE, Harnack O, Yasuda A, Wessels JM (2001) Adv Mater 13:1793
11. Harnack O, Ford WE, Yasuda A, Wessels JM (2002) Nano Lett 2:919
12. Keren K, Berman RS, Buchstab E, Sivan U, Braun E (2003) Science 302:1380
13. Monson CF, Woolley AT (2003) Nano Lett 3:359
14. Berti L, Alessandrini A, Facci P (2005) J Am Chem Soc 127:11216
15. Park SH, Prior MW, LaBean TH, Finkelstein G (2006) Appl Phys Lett 89:033901-1
16. Lin S, Li M, Dujardin E, Girard C, Mann S (2005) Adv Mater 17:2553
17. Zhong Z, Patskovskyy S, Bouvrette P, Luong JHT, Gedanken A (2004) J Phys Chem B 108:4046
18. Zhong Z, Luo J, Ang TP, Highfield J, Lin J, Gedanken A (2004) J Phys Chem B 108:18119
19. Zhong Z, Subramanian AS, Highfield J, Carpenter K, Gedanken A (2005) Chem Eur J 11:1473
20. Polavarapu L, Qing-Hua Xu (2008) Nanotechnology 19: 075601-1
21. Chapman GM, Bai H, Li C, Shi G (2009) Mater Chem Phys 114:120
22. Jovanovic SV, Simic MGJ (1986) J Phys Chem 90:974
23. Farha Al-Said SA, Hassanien R, Hannant J, Galindo MA, Pruneanu S, Pike AR, Houlton A, Horrocks BR (2009) Electrochem Commun 11:550
24. Girard P (2001) Nanotechnology 12:485
25. Lei CH, Das A, Elliot M, Macdonald JE (2004) Nanotechnology 15:627
26. Siggia S, Segal E (1953) Anal Chem 25:640

27. Bockrath M, Markovic N, Shepard A, Tinkham M, Gurevich L, Kouwenhoven LP, Wu MW, Sohn LL (2002) Nano Lett 2:187
28. Staii C, Johnson AT, Pinto NJ Jr (2004) Nano Lett 4:859
29. Zhou Y, Freitag M, Hone J, Staii C, Johnson AT, Pinto NJ, MacDiarmid AG (2003) Appl Phys Lett 83:3800
30. Brown S, Sarikaya M, Johnson E (2000) J Mol Biol 299:725
31. Naik RR, Stringer SJ, Agarwal G, Jones SE, Stone MO (2002) Nat Mater 1:169
32. Moores A, Goettmann F (2006) New J Chem 30:1121
33. Mie G (1908) Ann Phys (Leipz) 25:377
34. Liao JH, Zhang Y, Yu W, Xu LN, Ge CW, Liu JH, Gu N (2003) Colloids Surf A 223:177
35. Banfield JF, Welch SA, Zhang HZ, Ebert TT, Penn RL (2000) Science 289:751
36. Pong B-K, Lee J-Y, Trout BL (2005) Langmuir 21:11599